Electronic Supplementary Material (ESI) for Energy & Environmental Science.
This journal is © The Royal Society of Chemistry 2019

Supplementary Information

A universal solution processed interfacial bilayer enabling ohmic contact in organic and hybrid optoelectronic devices

Joel Troughton[1*], Marios Neophytou[1*], Nicola Gasparini[1], Akmaral Seitkhan[1], Furkan Isikgor[1], Xin Song[1], Yen-Hung Lin[2], Tong Liu[2], Hendrik Faber[1], Emre Yengel[1], Jan Kosco[1], Marek F. Oszajca[3], Benjamin Hartmeier[3], Michael Rossier[3], Norman A. Lüchinger[3], Leonidas Tsetseris[4], Henry Snaith[2], Stefaan De Wolf[1], Thomas Anthopoulos[1], Iain McCulloch[1,5], Derya Baran[1]

[1]King Abdullah University of Science and Technology (KAUST), KAUST Solar Center (KSC), Physical Sciences and Engineering Division (PSE), Thuwal, 23955-6900, Saudi Arabia

[2]Department of Physics, Clarendon Laboratory, University of Oxford, Parks Road, Oxford OX1 3PU, UK

[3]Avantama AG, Laubisrutistrasse 50, Stäfa, Switzerland

[4]Department of Physics, National Technical University of Athens, 15780 Athens, Greece

[5] Department of Chemistry, Imperial College London, SW7 2AZ, UK

Experimental details

TiO_2 and Nb-TiO_2 nanoparticle synthesis

The dry TiO_2 and Nb-TiO_2 nanopowder was prepared by flame spray synthesis using a precursor solution of titanium isopropoxide (Sigma Alrdrich) and niobium 2-ethylhexanoate (ABCR) in 2-ethylhexanoic acid; the solution was diluted with 30 wt% tetrahydrofuran (THF). The precursor then was fed (7 ml min^{-1} to a spray nozzle, dispersed by oxygen (15 l min^{-1}) and ignited by a premixed methane-oxygen flame (CH_4: 1.2 l min^{-1} and O_2: 2.2 l min^{-1}, Both Messer AG). The off-gas was filtered through a steel mesh filter (20 μm mesh size) by a vacuum pump at about 20 m^3 h^{-1}. The obtained dry TiO_2 and Nb-TiO_2 nano powder was collected from the filter mesh.

A stable suspension (Batch #10174) was prepared by dispersing 2.5 wt% nanopowder in a mixture of 50 wt% 1-butanol and 50 wt% 2-butanol by using an undisclosed dispersant (proprietary information of Avantama AG).

Transmission electron microscopy characterization

For cross-sectional TEM images, a thin lamella from the sample was first prepared with a focused ion beam (FIB) in a scanning electron microscope (Helios 400s, FEI) equipped with a nanomanipulator (Omniprobe, AutoProbe300). The sample's surface was protected by sequential layers of carbon and platinum deposited under the electron and ion beams. The bulk of the sample was milled with a Ga ion beam to reach the depth of ca. 8-10 μm. A 'U-cut' was made with the FIB and the lamella was extracted from the bulk according to the lift-out method. The lamella, attached to a copper TEM grid, was then thinned down with the FIB at 30 kV and sequentially reducing current in the range of 2.8 nA to 93 pA. The lamella was polished with the FIB at low voltages (5 and 2 kV) to remove any possible contamination. The top-view and cross-sectional images were acquired with the TEM (Titan 80-300, FEI) at 300 kV operating voltage.

Ultraviolet photo-electron spectroscopy (UPS) characterization

UPS measurements were performed in a multi-probe UHV chamber (Omicron) equipped with an ISE-5 cold cathode ion gun for ion sputter cleaning (Ar^+) at a base pressure of 10^{-9} mbar. The UPS source was a non-attenuated He (I) discharge lamp with an excitation energy of 21.21 eV. Spectra were recorded with an analyzer spot of 60 μm diameter at 5 eV pass energy and a bias of -9.77eV.

Electron-only device fabrication

Pre-patterned ITO-coated glass (10 Ohm/sq, Xinyan Glass) was cleaned through sequential sonication in detergent (Hellmanex 3), DI water, acetone and isopropyl alcohol before undergoing 10 minutes of oxygen plasma treatment. A thin layer of SnO_2 was deposited by spin-coating a 2.5 wt% colloidal suspension of SnO_2 in H_2O (Alfa Aesar) onto ITO substrates at 4000 rpm for 30 seconds followed by drying at 140°C for 10 minutes. A $CH_3NH_3PbI_3$ perovskite precursor solution was prepared by dissolving 1.25 M lead iodide (TCI) and 1.25 M methylammonium iodide (Greatcell solar) in a 4:1 by volume solution of n,n-dimethylformamide (DMF) and dimethyl sulfoxide (DMSO). This perovskite precursor solution was spin-coated onto the coated substrates inside a N_2-filled glovebox at 4000 rpm for 30 seconds, with 150 µl chlorobenzene poured onto the spinning sample 10 seconds from the end of the cycle. Perovskite films were annealed at 100°C for 30 minutes. To form a PCBM layer, a 20 mg ml^{-1} solution of PCBM (Solenne BV) in chlorobenzene was spin-coated onto the perovskite films at 1300 rpm for 30 seconds.

To form the interfacial bilayer, a 2.5 wt% suspension of TiO_2 or Nb-TiO_2 nanoparticles in butanols (Avantama) was diluted to 0.4 wt% in 1-butanol and spin-coated onto the PCBM at 5000 rpm for 10 seconds. If necessary, a secondary layer of bathocuproine was deposited using the same parameters (0.5 mg ml^{-1} in anhydrous ethanol). 100 nm of silver metallic electrode was evaporated at 10^{-6} mbar.

$MAPbI_3$ Perovskite solar cell fabrication

ITO-coated glass was cleaned in the same manner as for electron-only devices. For NiOx-containing devices, a solution containing 0.3 M nickel acetate tetrahydrate and 0.3 M ethanolamine in 2-methoxyethanol and was spin-coated onto the glass substrates at 4000 rpm for 30 seconds before annealing at 300°C for 20 minutes to form a NiOx film.

$CH_3NH_3PbI_3$, PCBM, interfacial bilayers and metal electrodes were deposited in the same manner as for electron-only devices.

Mixed cation & halide perovskite solar cell fabrication

To form the mixed-cation lead mixed-anion perovskite precursor solutions, CsI, FAI, PbI_2 and $PbBr_2$ were prepared in the way corresponding to the exact stoichiometry for the desired $Cs_{0.05}(FA_{0.83}MA_{0.17})_{0.95}PbI_{2.7}Br_{0.3}$ compositions in a mixed organic solvent of anhydrous DMF and DMSO at the ratio of DMF : DMSO = 4 : 1. The perovskite precursor concentration used was 1.40 M.

For the hole transporting material, poly(4-butylphenyl-diphenyl-amine) (Poly-TPD, 1-Material) was dissolved in toluene in a concentration of 1 mg/mL along with 20 wt% of 2,3,5,6-Tetrafluoro-7,7,8,8-tetracyanoquinodimethane (F4-TCNQ, Lumtec). For the electron transporting materials, PCBM and BCP were dissolved in chlorobenzene: 1,2-dichlorobenzene (3:1 in volume) and isopropanol at a concentration of 20 and 0.5 mg mL^{-1}, respectively. For preparing the doped PCBM, an n-dopant 4-(2,3-Dihydro-1,3-dimethyl-1H-benzimidazol-2-yl)-N,N-dimethylbenzenamine (N-DMBI, Sigma-Aldrich) was dissolved using the same solvent as for PCBM at the desirable molar ratio to $PC_{61}BM$.

The deposition of perovskite layers was carried out using a spin coater in a nitrogen-filled glove box with the following processing parameters: starting at 1000 rpm (ramping time of 4 sec) for 10 sec and then 6000 rpm (ramping time of 6 sec from 1000 rpm) for 35 sec. 10 sec before the end of the spinning process, a solvent-quenching method was used by dropping 300 µL toluene onto the spinning substrates.

The mixed-cation & mixed anion perovskite solar cells were fabricated using TEC-7 fluorine doped tin oxide coated glass substrates. After the substrate cleaning procedure, F4-TCNQ doped Poly-TPD was deposited by dispensing the as-prepared organic solution onto a spinning substrate at 2000 rpm for 20 sec, followed by thermal annealing at 130 °C for 10 minutes in ambient air. The deposition of perovskite layers was carried out using a spin coater in a N_2-filled glove box with the following processing parameters: starting at 1000 rpm (ramping time of 4 sec) for 10 sec and then 6000 rpm (ramping time of 6 sec from 1000 rpm) for 35 sec. 10 sec before the end of the spinning process, a solvent-quenching method was used by dropping 300 µL toluene onto the spinning substrates. The thermal annealing process (100 °C for 60 minutes) was then carried out for the formation of the perovskite layer.

For the mixed cation & anion perovskite solar cells, only the perovskite absorber layer and the electron-transporting layers were processed in a nitrogen-filled glovebox; the rest of the fabrication as well as the incomplete devices were processed and handled in ambient air. Finally, the perovskite solar cells were completed by thermal evaporation of 70 nm of silver contacts under high vacuum (10^{-5}–10^{-6} mbar).

Organic solar cell fabrication

ITO glass was prepared in an identical fashion to the perovskite solar cells. A layer of PEDOT:PSS (Heraeus AL4083) was spin-coated onto glass substrates at 5000 rpm for 60 seconds before annealing at 140°C for 10 minutes. PTB7-Th and IEICO-4F (both 1-material) were dissolved separately in chlorobenzene at 20 mg ml^{-1} before being mixed in the volume ratio 1:2. This active layer solution was spin-coated onto the PEDOT:PSS substrates at 1000 rpm for 60 seconds before annealing at 130°C for 10 minutes. The interfacial bilayer and Ag electrode was deposited in the same manner as described for electron-only devices.

Organic light emitting diode fabrication

PEDOT:PSS-coated ITO glass was prepared as for organic solar cells. A solution of poly(9,9-di-n-octylfluorenyl-2,7-diyl) : poly(9,9-dioctylfluorene-alt-benzothiadiazole) (F8:F8BT, 19:1 by weight, synthesis detailed below) was dissolved in toluene at 10 mg ml^{-1} and spin-coated at 2000 rpm for 60 seconds before annealing at 80°C for 10 minutes. The interfacial bilayer and metal electrode were deposited in the same manner as described for perovskite solar cells.

Thin-film transistor device fabrication & characterization

The precursors for the film formation of In_2O_3 and ZnO were respectively prepared from indium nitrate hydrate in 2-methoxyethanol (both purchased from Sigma Aldrich) at a concentration of 30 mg ml^{-1} and from ZnO powder (Sigma Aldrich) dissolved in ammonium hydroxide (50% v/v aqueous solution, Alfa Aesar) at a concentration of 10 mg ml^{-1}. Silicon substrates with a thermally grown 100 nm thick SiO_2 layer served as combined global gate electrode and dielectric material. Consecutive ultrasonication steps in deionized water, acetone and isopropanol for 10 minutes each were carried out to clean the substrates, followed by 10 minutes of UV/ozone treatment directly before the semiconductor deposition via spin coating. For both layers, a spin speed of 4000 rpm was used over 30 secs with a subsequent annealing step at 210 °C for 30 min. Spin coating and annealing were carried out inside a nitrogen filled glove box in case of In_2O_3 and in ambient air for ZnO. The Nb-TiO_2 and BCP interfacial bilayers were processed in the same manner as previously described. Finally, TFT fabrication was concluded by deposition and patterning of a 40 nm film of silver via thermal evaporation through shadow masks to form source and drain electrodes of channel width $W = 1000$ µm and channel length $L = 30$ µm.

For the low voltage transistors, glass substrates were cleaned in the same manner as described above, followed by the deposition of 100 nm thick Al gate electrodes. To form the self-assembled monolayer (SAM) dielectric, the gate electrodes were first subjected to a 10 min UV/ozone treatment, followed by immersion into an isopropanol solution containing 7 mg ml^{-1} of phosphonohexadecanoic acid (PHDA, Sigma Aldrich) for 36 hours. Afterwards the substrates were flushed with excess isopropanol and dried on a hotplate for 5 minutes at 60 °C. The subsequent deposition of metal oxide semiconductors, interlayers and silver source/drain electrodes were identical to the description above.

All electrical measurements were carried out inside a nitrogen filled glovebox using a Keysight B2912A source meter. The change in interfacial trap density ΔN_{tr} for devices with and without the Nb-TiO_2 + BCP bilayer was calculated according to:

$$\Delta N_{tr} = \frac{C_i|\Delta V_{TH}|}{e}$$

with the geometric capacitance of the gate dielectric C_i, the shift in threshold voltage ΔV_{TH} and the elementary charge e.

Density Functional Theory calculations

Results on Nb-doped TiO_2 and Ag surfaces were obtained with the plane wave-based code Quantum Espresso,[1] ultrasoft pseudopotentials,[2] and the Perdew-Wang generalized gradient approximation exchange-correlation (xc) functional.[3] Results on isolated BCP molecules, on the other hand, were obtained with the quantum chemistry code NWChem,[4] the hybrid B3LYP xc-functional, [5,6] and the DZVP localized orbital basis.[7] To visualize the structures and the frontier orbitals we used the software VESTA.[8]

Solar cell characterization

Both perovskite and organic solar cells were tested using a >AAA rated LED solar simulator (WaveLabs Sinus-70) calibrated against a NIST traceable silicon reference. For perovskite devices, current-voltage measurements were performed in both scan directions from -0.1V to 1.2V with a 50mV/s scan speed. Organic solar cells were measured from -0.1V to 1.0V at the same scan speed. The active area of solar cells was defined by the intersection between perpendicular ITO and metal “finger” electrodes, as well as with a metal shadow mask with aperture area 0.1 cm^2

External quantum efficiency measurements were performed using an Enlitech QE-R EQE system calibrated against a NIST-traceable Si detector. Monochromated light was chopped at 210 Hz and signal processed using a lock-in amplifier to eliminate the influence of stray light. Measurements were taken at 10 nm wavelength intervals between 300 nm and 850 nm for perovskite devices and between 300 nm and 1050 nm for organic solar cells.

For operational stability measurements, solar cells were loaded into a test chamber continuously purged with N_2 gas and placed on a temperature controlled (35°C) platform underneath a metal halide arc lamp with intensity calibrated to 1 sun using a KG-5 filtered reference cell. Solar cells were continuously irradiated, and no UV or IR cut-off filters were used. The spectrum of the lamp used for stability measurements can be seen in Figure S20. J-V scans from +1.3 V to -0.1 V at 50 mV s^{-1} were performed at 10 minute intervals. Between measurements, devices were held at open-circuit.

TPC characterization

For transient photocurrent (TPC) measurements, a 405 nm laser diode driven by a function generator was used to generate 100 µs light pulses. The current response was amplified with a transimpedance amplifier and recorded with a digital oscilloscope.

OLED characterization

Current-luminance-voltage characterization of the devices were conducted simultaneously using a Keysight B2912A source meter and Konika Minolta Luminance Meter LS-150. EL spectra were collected using an integrating sphere (Thorlabs IS236A) connected to an Ocean Optics (QE65000) spectrometer through an optical fiber. Radiated power of EL and operational lifetime measurements were carried out using an integrating sphere photodiode power sensor (Thorlabs S142C) in parallel with the current measurements from source meter. All measurements were taken from the front face of the device using a home-built characterization system in dark under nitrogen atmosphere. Home-built characterization software was used for measurements to minimize the time delay between measurement points.

F8/F8BT

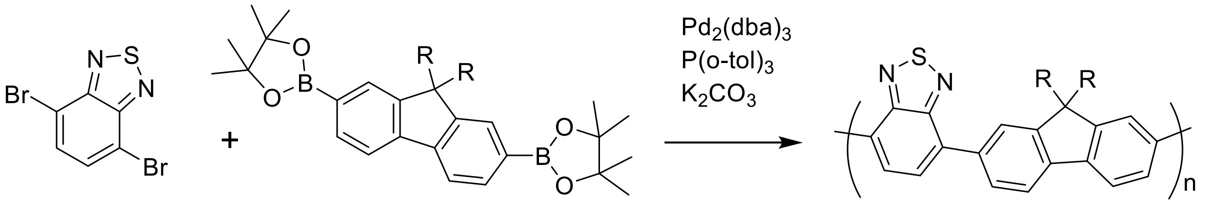

Scheme 1: F8BT synthesis

F8BT synthesis

F8BT was synthesized from its monomers using a modified literature procedure (Scheme 1).[10] All solvents were thoroughly degassed with nitrogen prior to use. A solution of potassium phosphate (0.529 g, 2.49 mmol) in 2 mL water and 0.5 mL dioxane was added to a mixture of 9,9-Dioctyl-9H-fluorene-2,7-diboronic acid bis(pinacol) ester (400 mg, 0.623 mmol), 4,7-Dibromobenzo[c]-1,2,5-thiadiazole (183 mg, 0.623 mmol), Tris(dibenzylideneacetone)dipalladium(0) ($Pd_2(dba)_3$) (5.7 mg, 6.22 µmol, 2 mol% Pd), and tri(o-tolyl)phosphine ($P(o\text{-}tol)_3$), (11.4 mg, 37.5 µmol, 6 mol%) in toluene (2 mL). The mixture was stirred vigorously inside a sealed microwave vial for 24 h at 110 °C. The contents were removed, and washed by consecutive Soxhlet extractions with methanol, acetone, and hexane, each for 24 h. The polymer was extracted with chloroform, concentrated under reduced pressure, and precipitated into methanol. The yellow precipitate was filtered to obtain F8BT (Mn = 39.6 kD Mw = 84.4 kD, PDI = 2.13, 507 mg 87% yield).

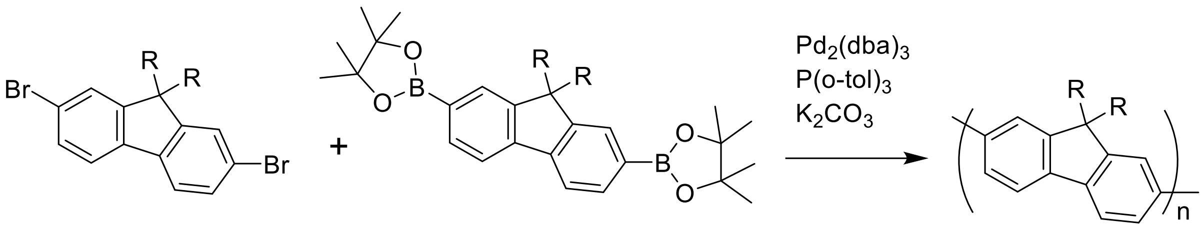

Scheme 2: PFO synthesis

PFO (F8) synthesis

PFO was synthesised from its monomers using a modified literature procedure (Scheme 2).[10] All solvents were thoroughly degassed with nitrogen prior to use. A solution of potassium phosphate (0.529 g, 2.49 mmol) in 2 mL water and 0.5 mL dioxane was added to a mixture of 9,9-Dioctyl-9H-fluorene-2,7-diboronic acid bis(pinacol) ester (400 mg, 0.623 mmol), 9,9-Dioctyl-2,7-dibromofluorene (342 mg, 0.623 mmol), Tris(dibenzylideneacetone)dipalladium(0) ($Pd_2(dba)_3$) (5.7 mg, 6.22 µmol, 2 mol% Pd), and tri(o-tolyl)phosphine ($P(o\text{-}tol)_3$), (11.4 mg, 37.5 µmol, 6 mol%) in toluene (2 mL). The mixture was stirred vigorously inside a sealed microwave vial for 24 h at 110 °C. The contents were removed, and washed by consecutive Soxhlet extractions with methanol, acetone, and hexane solvents, each for 24 h. The polymer was extracted with chloroform, concentrated under reduced pressure, and precipitated into methanol. The white precipitate was filtered to obtain PFO (Mn = 39.6 kD Mw = 84.4 kD, PDI = 2.13, 507 mg 82% yield).

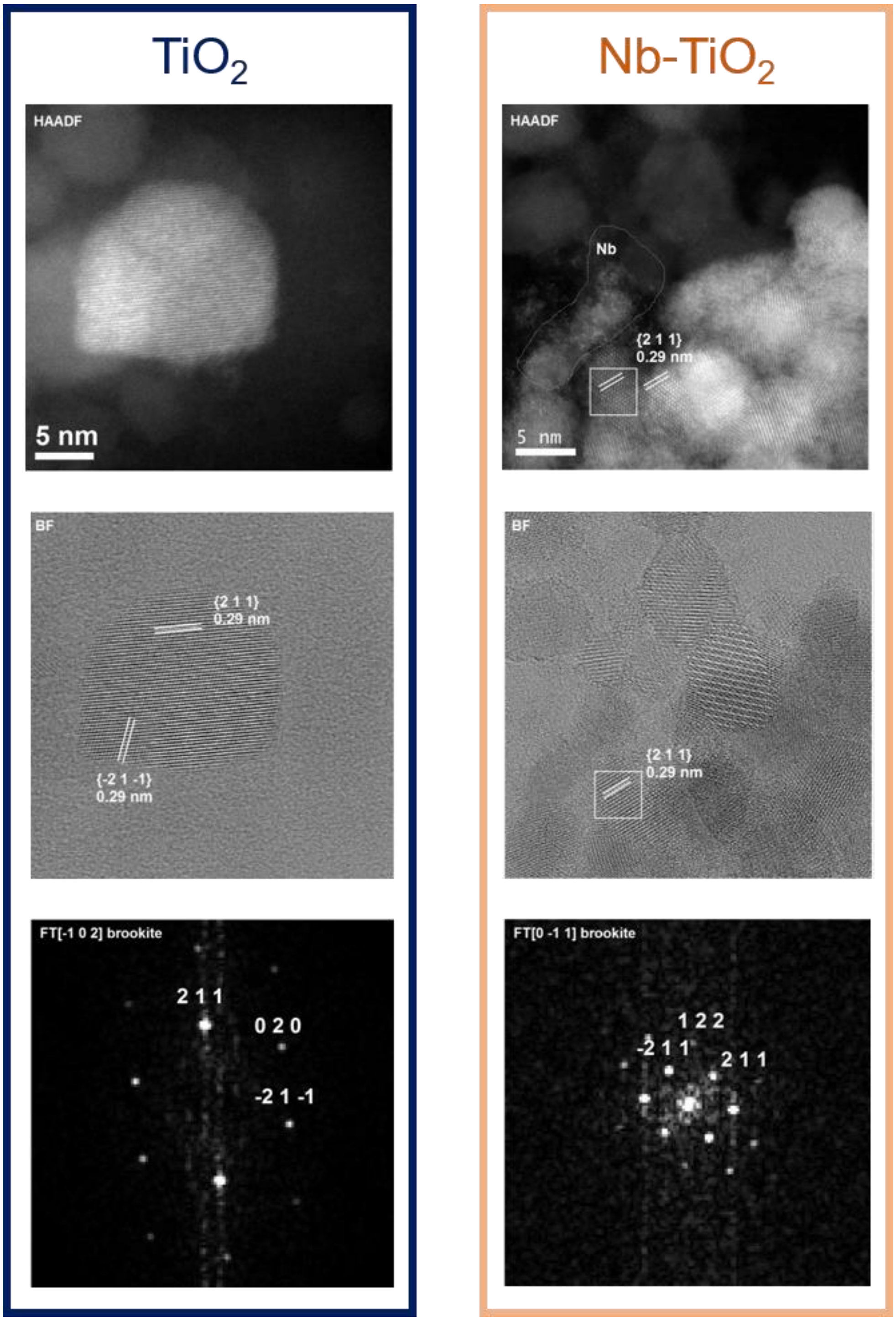

Figure S1. TEM micrographs of pristine TiO_2 and Nb-doped TiO_2 nanoparticles in light and dark field. Lattice spacing in both instances is measuredly identical owing to the ionic radius similarity between Nb^{5+} and Ti^{4+}, allowing substitutional doping with no significant lattice distortion.

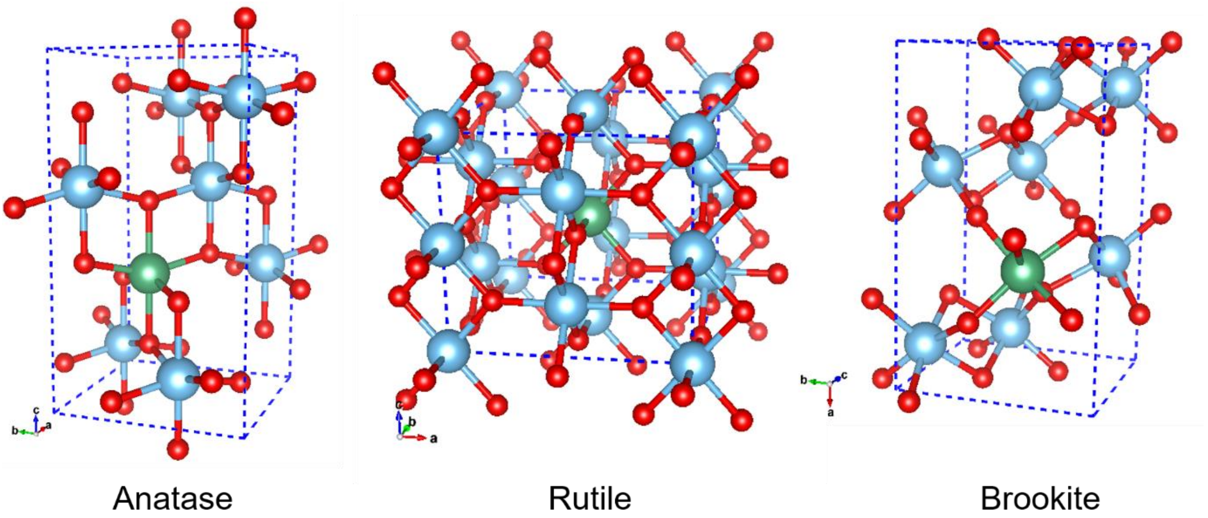

Figure S2. Nb-TiO_2 polymorphs. Doping of 1 Nb atom (green) per 8 Ti sites (blue) (x_{Nb} = 0.125). Doping with Nb changes the calculated brookite lattice parameters from a = 9.262 Å, b = 5.501 Å, c = 5.173 Å in the undoped case to a = 9.300 Å, b = 5.526 Å, c = 5.217 Å for Nb-TiO_2. Even at this high doping concentration, changes in a, b, c are minimal (<1%).

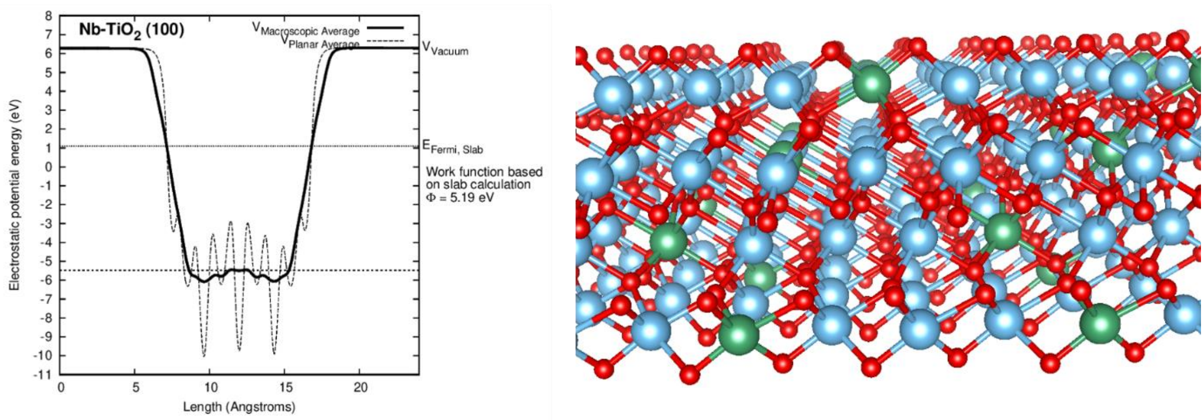

Figure S3. Calculated electrostatic potential energy (left panel) for a (100) surface (right panel, Ti: blue, Nb: green, O: red spheres) of Nb-doped brookite TiO_2 with Nb concentration x_{Nb} = 0.125. The calculated work function for this surface of Nb-TiO_2 is 5.19 eV

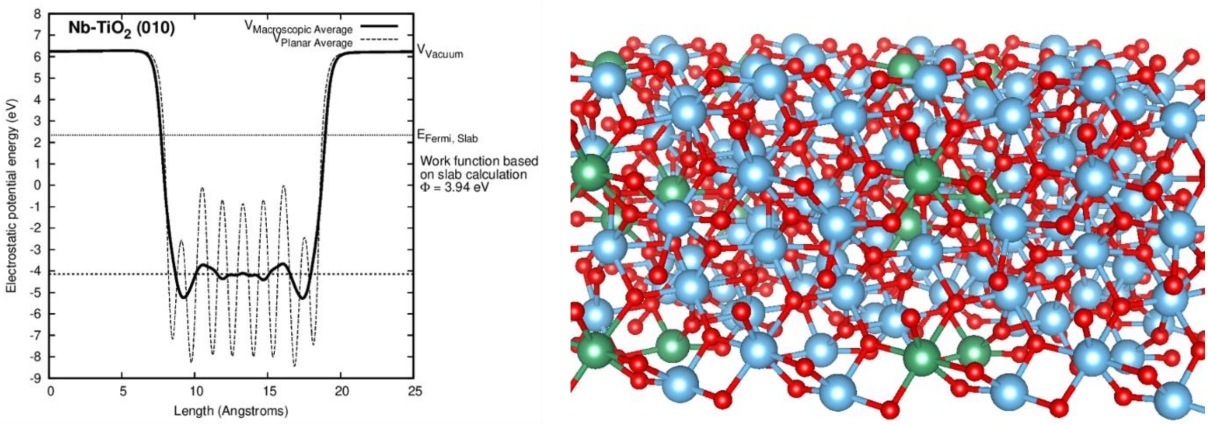

Figure S4. Calculated electrostatic potential energy (left panel) for a (010) surface (right panel, Ti: blue, Nb: green, O: red spheres) of Nb-doped brookite TiO_2 with Nb concentration $x_{Nb} = 0.125$. The calculated work function is for this surface of Nb-TiO_2 is 3.94 eV

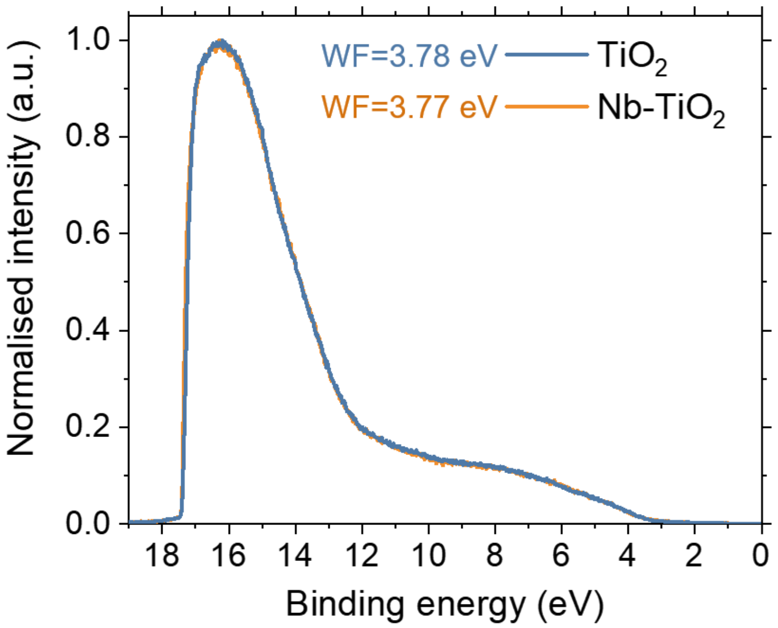

Figure S5. Work function of pristine TiO_2 and Nb-TiO_2 nanoparticles measured using ultraviolet photoelectron spectroscopy (UPS). The work function of TiO_2 is unchanged upon the inclusion of Nb around 3.8 eV

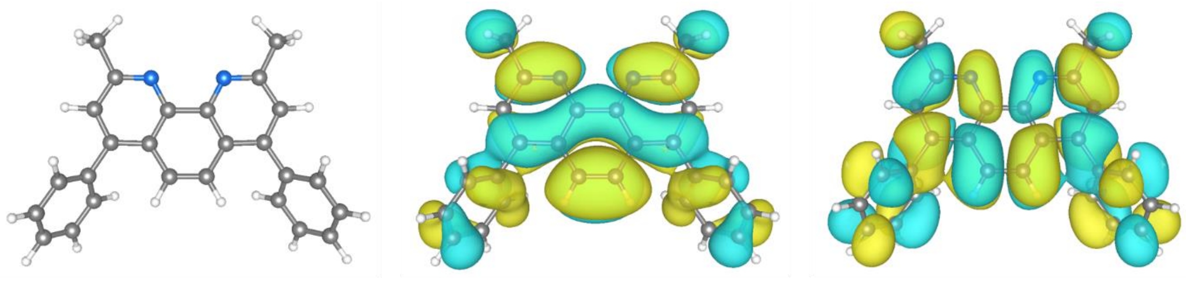

E_{HOMO} = -6.07 eV

E_{LUMO} = -1.62eV

Figure S6. Simulated Highest Occupied (HOMO, -6.07 eV) and Lowest Unoccupied (LUMO, -1.62 eV) Molecular Orbitals of a bathocuproine (BCP) molecule (left panel).

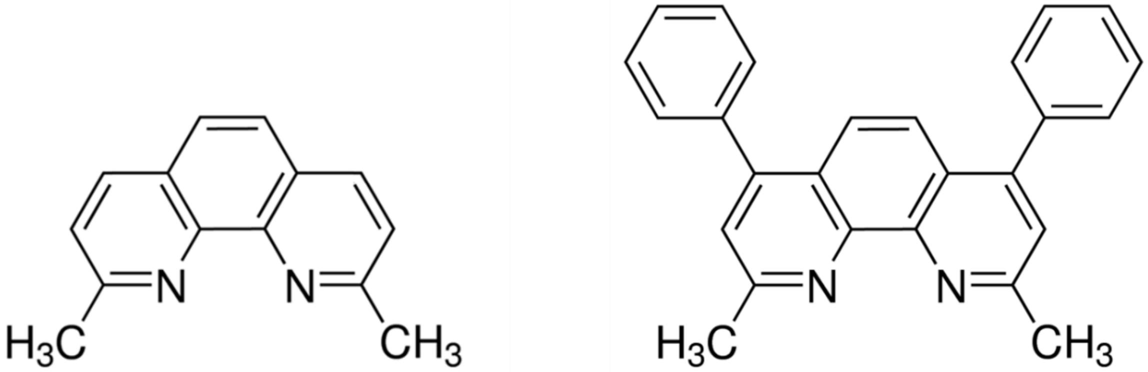

Neocuproene

Bathocuproene

Figure S7. Chemical structures of neocuproene (left) and bathocuproene (right). The metal-bonding nitrogen sites in both molecules are identical

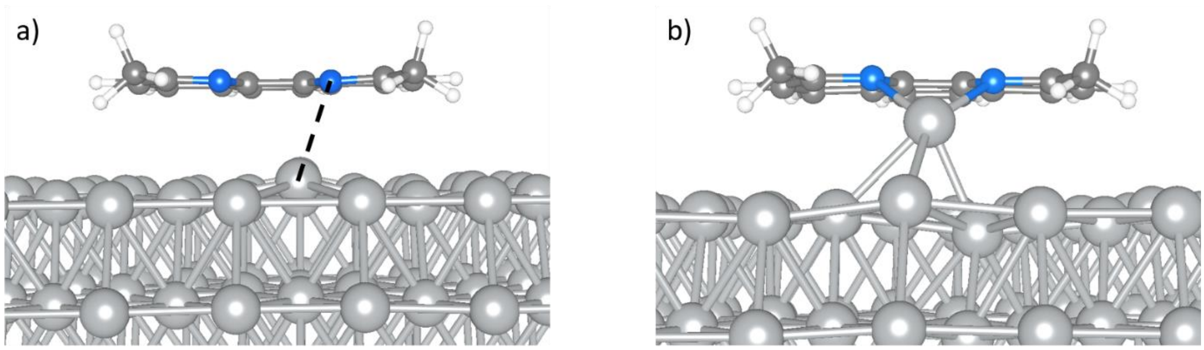

Ag-111 pristine surface

Ag-111 surface with Ag adatom

Figure S8. Adsorption of a neocuproene molecule on a Ag-111 surface (a) and Ag-111 surface with additional Ag adatom (b). The left configuration has an adsorption energy (E_b) of 2.15 eV. Although no direct bond is formed between NCP and Ag, the interaction between the molecule and the underlying surface is strong leading to a reduced Ag-N distance of 2.85 Å (dashed line). In the configuration (b), E_b is even larger (2.82 eV) due to the Ag-N bonds formed between the NCP molecule and Ag adatom.

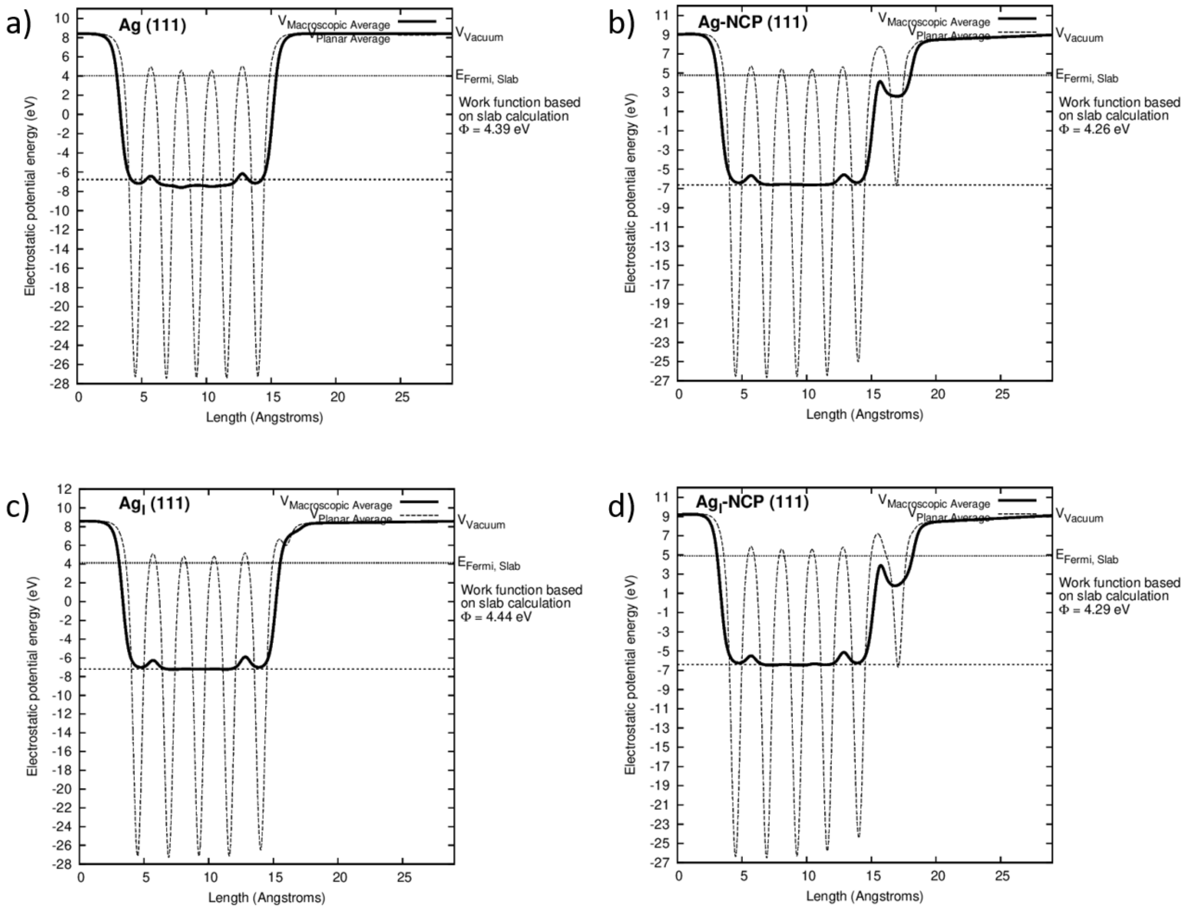

Figure S9. Electrostatic potential energies and work functions for (a) pristine Ag-111 surface, (b) configuration of Figure. S8a, (c) Ag-111 surface with an Ag adatom, (d) configuration of Figure. S8b.

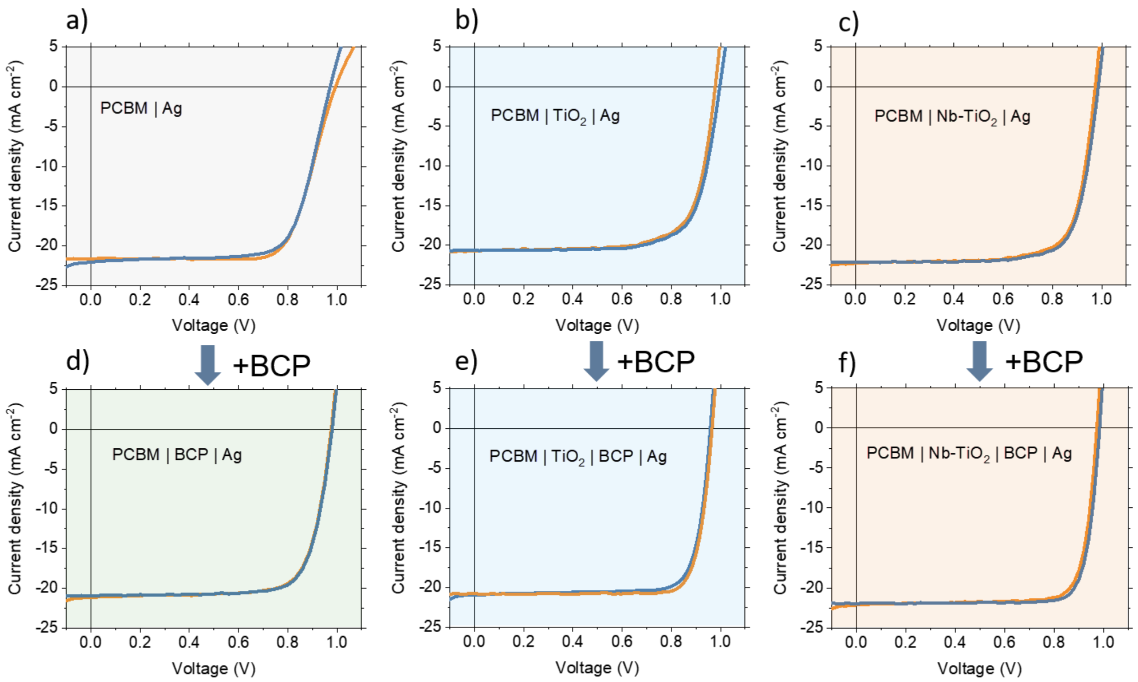

Figure S10: Current-voltage curves in both scan directions for perovskite solar cells employing different interfacial layers between PCBM and Ag electrode. Orange traces correspond to scans from V_{OC} to J_{SC} (“reverse”) whereas blue traces illustrate the opposite direction (“forward).

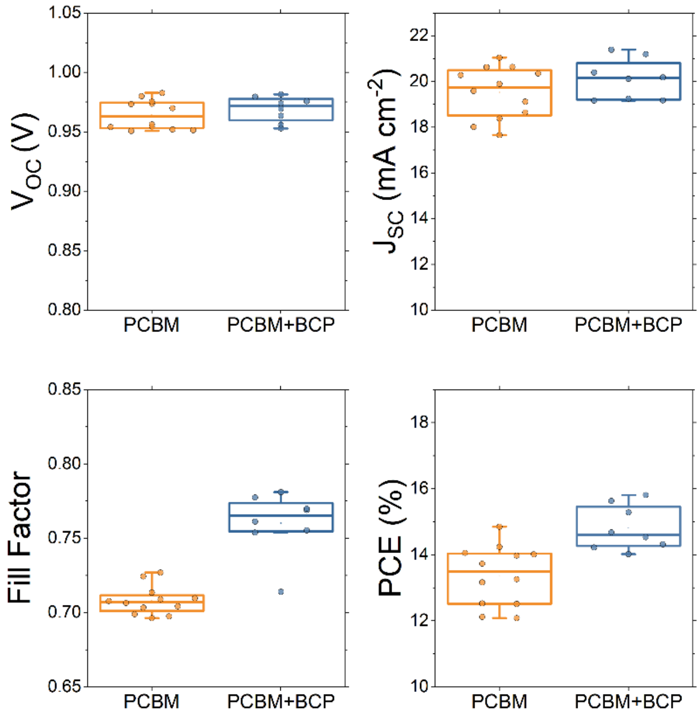

Figure S11: Current-voltage parameters for perovskite solar cells employing no interfacial layer between PCBM and Ag electrode (orange) and a BCP interlayer (blue). Data from a total of 20 devices (12x “PCBM”, 8x “PCBM+BCP”).

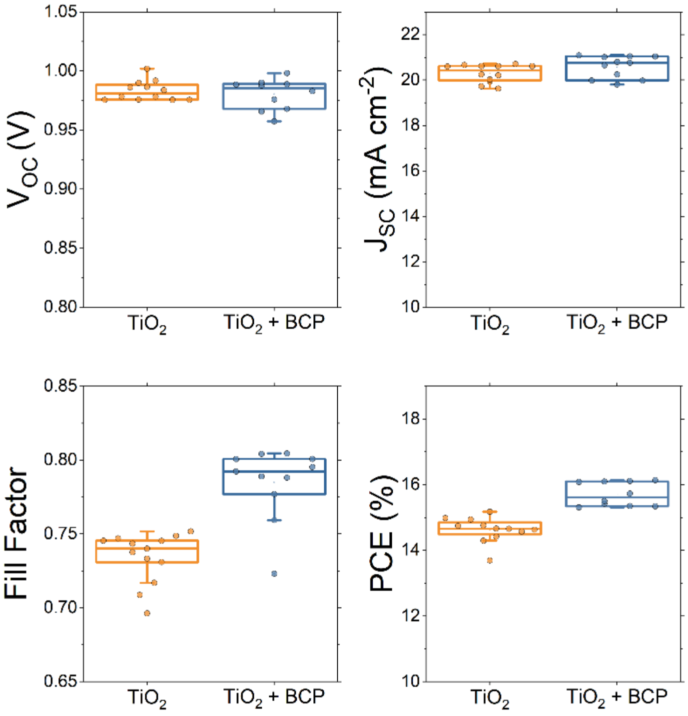

Figure S12: Current-voltage parameters for perovskite solar cells employing a TiO_2 interfacial layer between PCBM and Ag electrode (orange) and a TiO_2 & BCP bilayer at the same interface (blue). Data from a total of 22 devices (12x “TiO_2”, 10x “TiO_2+BCP”).

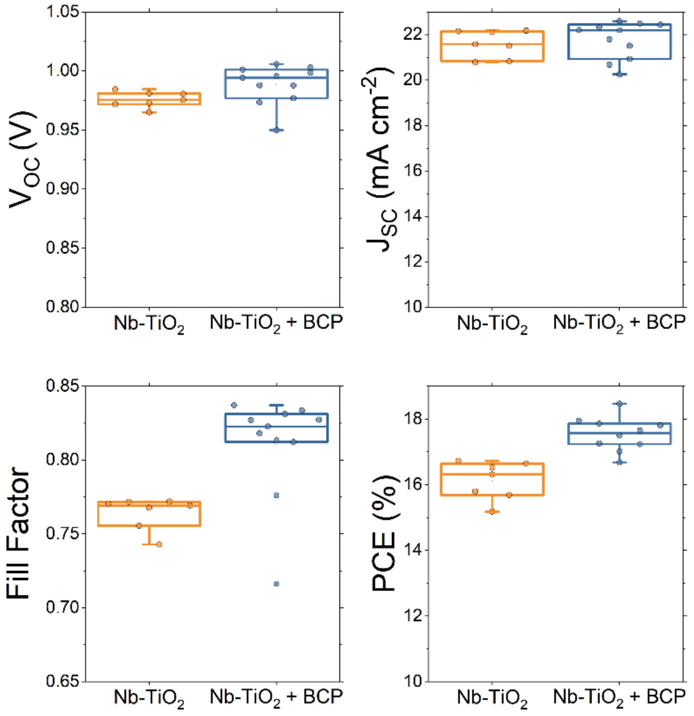

Figure S13: Current-voltage parameters for perovskite solar cells employing a Nb-TiO_2 interfacial layer between PCBM and Ag electrode (orange) and a Nb-TiO_2 & BCP bilayer at the same interface (blue). Data from a total of 18 devices (7x “Nb-TiO_2”, 11x “Nb-TiO_2+BCP”).

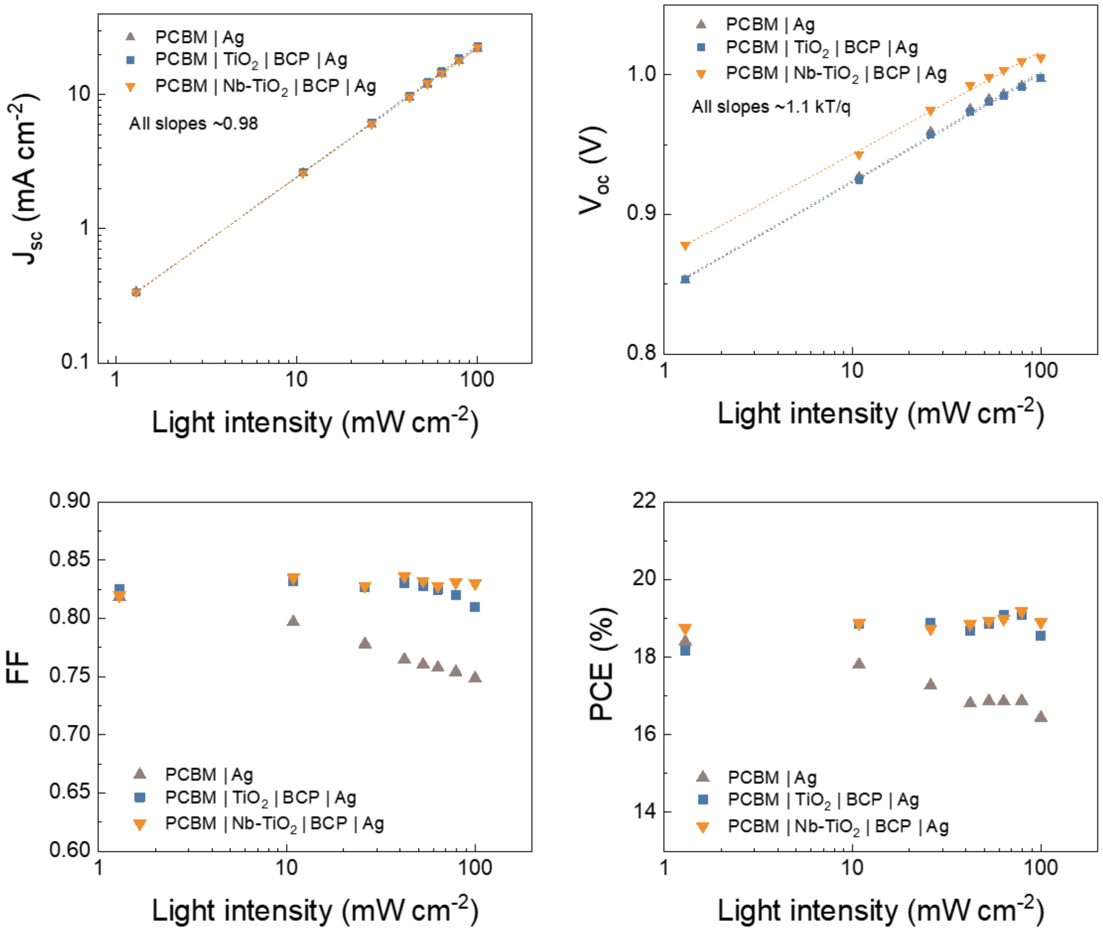

Figure S14. Current-voltage parameters as a function of light intensity for perovskite solar cells employing different interfacial layers.

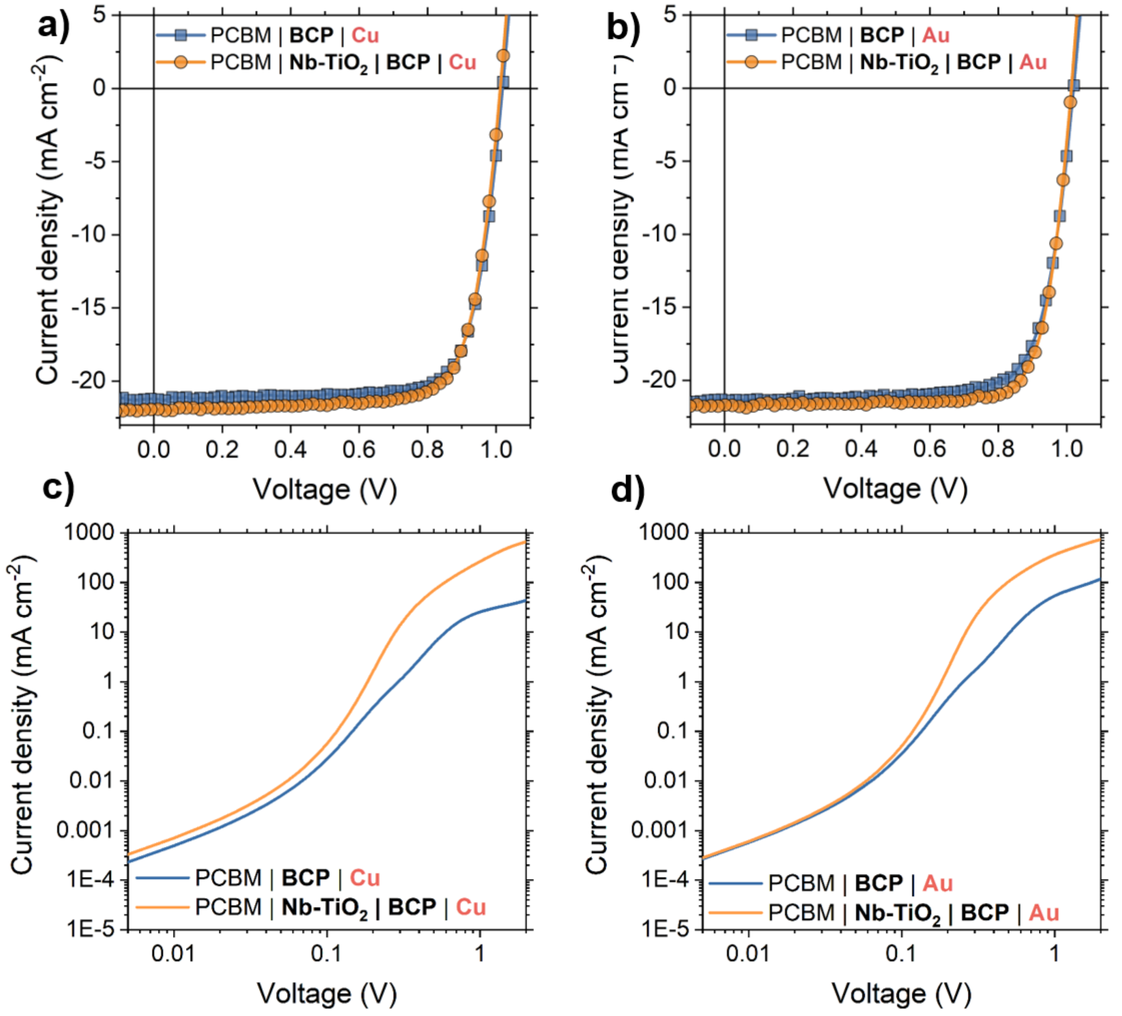

Figure S15. Current-voltage curves for perovskite solar cells employing different interfacial layers with copper (a) and gold (b) metal electrodes. c-d) show electron-only devices using the same layers and electrodes.

ITO | NiOx | $MAPbI_3$ | …	Electrode	J_{SC} (mA cm^{-2})	V_{OC} (V)	FF	PCE (%)
PCBM | **BCP** | …	Cu	21.2	1.02	0.77	16.6
PCBM | **Nb-TiO_2 | BCP** | …		21.9	1.02	0.76	17.0
PCBM | **BCP** | …	Au	21.3	1.02	0.76	16.5
PCBM | **Nb-TiO_2 | BCP** | …		21.7	1.01	0.79	17.4

Table S1. Solar cell performance metrics for the devices show in Figure S15 (a-b)

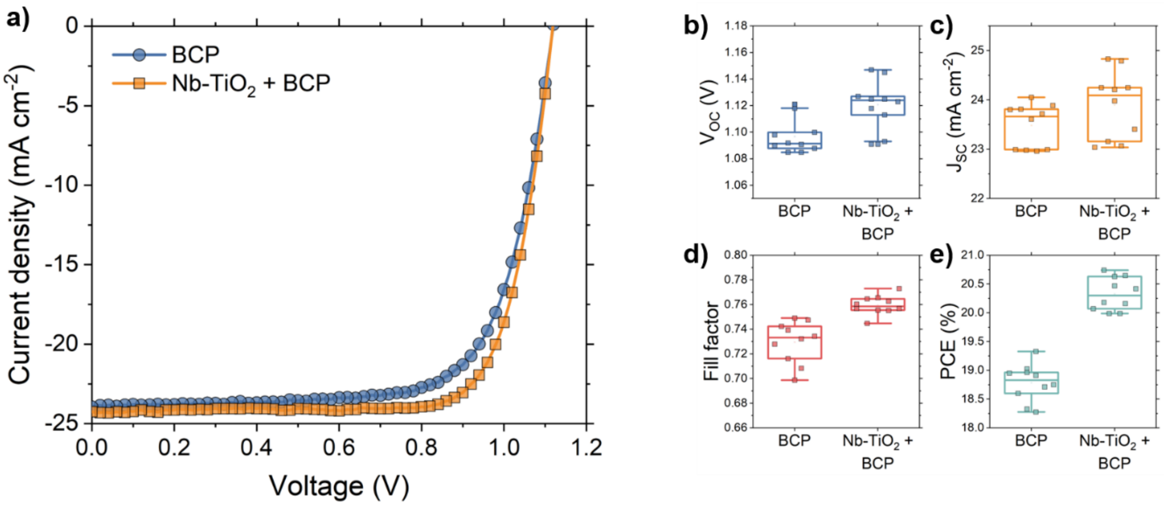

Figure S16. a) Current-voltage curves for champion $MAPbI_3$ devices employing a PTAA hole transport layer, as well as BCP or Nb-TiO_2/BCP bilayer interfacial layers. b-e) Box plots of current-voltage parameters between interfacial layers (n=10 for each device set).

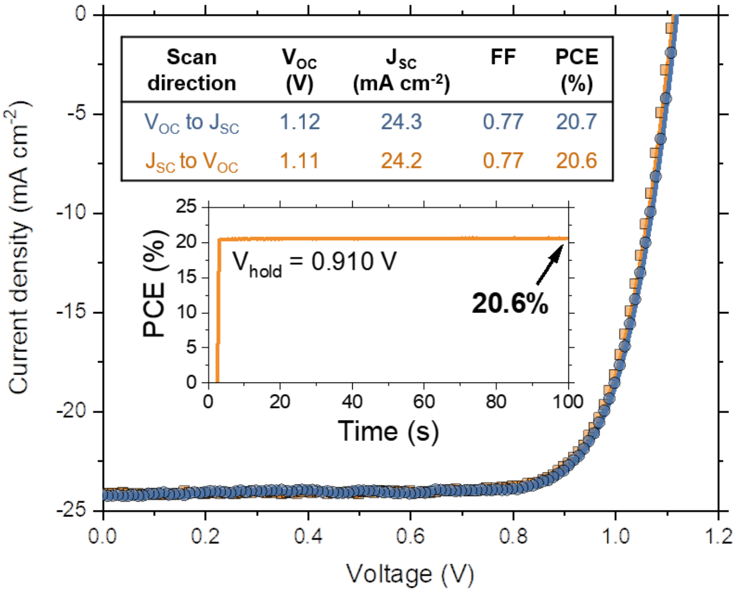

Scan direction	V_{OC} (V)	J_{SC} (mA cm^{-2})	FF	PCE (%)
V_{OC} to J_{SC}	1.12	24.3	0.77	20.7
J_{SC} to V_{OC}	1.11	24.2	0.77	20.6

Figure S17. Current-voltage curves for “hero” perovskite solar cell employing a PTAA HTL, $MAPbI_3$ perovskite, Nb-TiO_2/BCP interfacial bilayer. The sub-figure shows the stabilized PCE after 100 seconds held at the maximum power point.

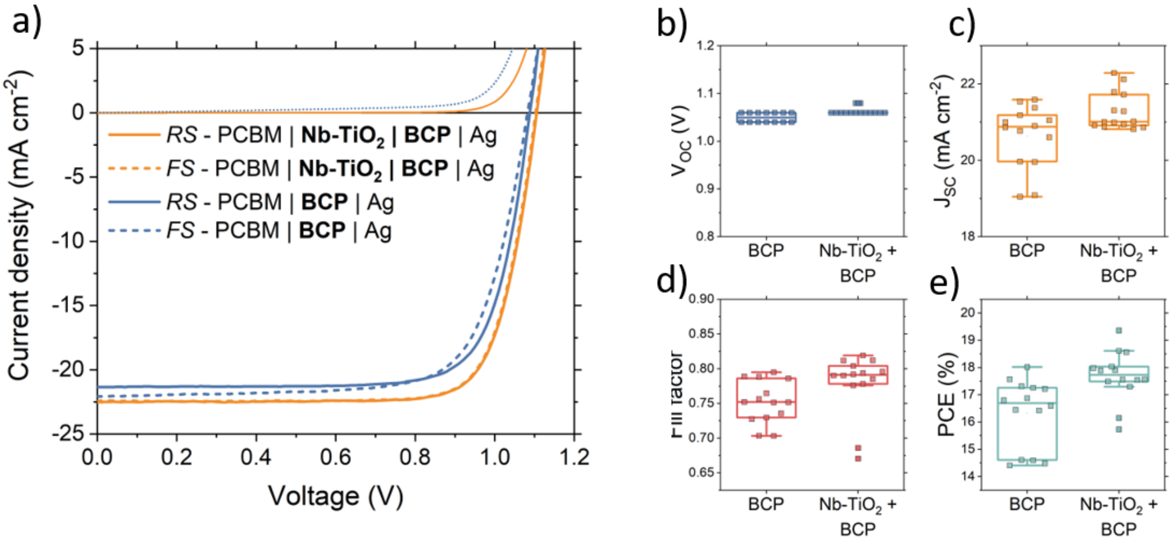

Figure S18: **a)** Current-voltage curves in both scan directions for perovskite devices comprising a Poly-TPD HTL and $Cs_{0.05}(FA_{0.83}MA_{0.17})_{0.95}PbI_{2.7}Br_{0.3}$ perovskite absorber. Solid lines denote the “reverse” scan direction whereas dashed lines denote the “forward” scan direction. **b-e)** Box plots of current-voltage parameters between interfacial layers (n=14 for each device set).

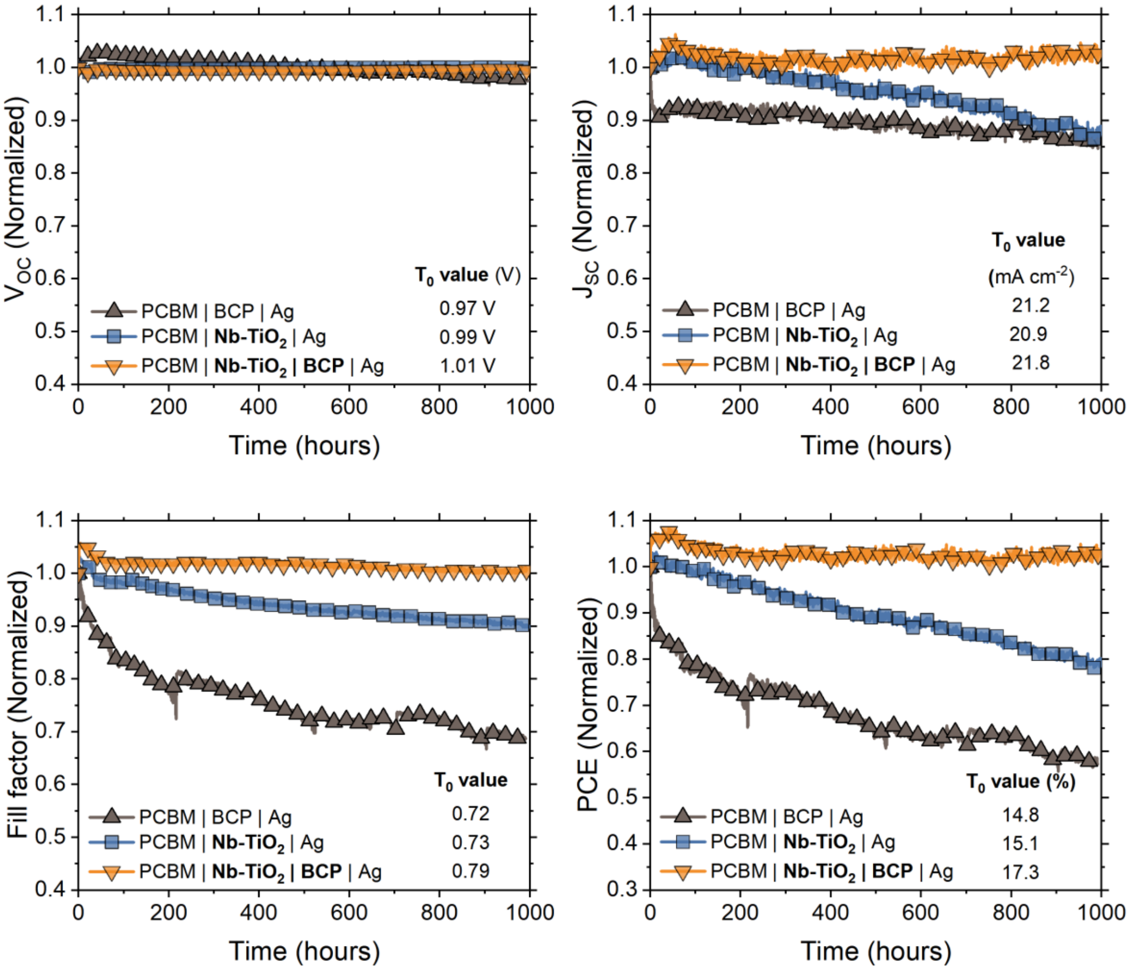

Figure S19. Current-voltage curve parameters for ‘*p-i-n*’ MAPbI$_3$ perovskite solar cells employing different interfacial bilayers over time. Devices were exposed to full spectrum 1 sun illumination, as illustrated in Figure S20. A nitrogen atmosphere was used, and average cell temperature was recorded at 35°C. Initial values are stated within boxes as “T$_0$”.

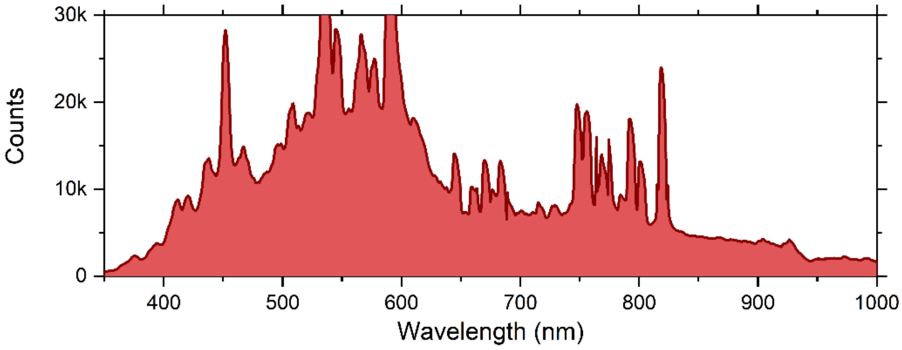

Figure S20. Output spectrum of the metal-halide discharge lamp used for continuous stability testing.

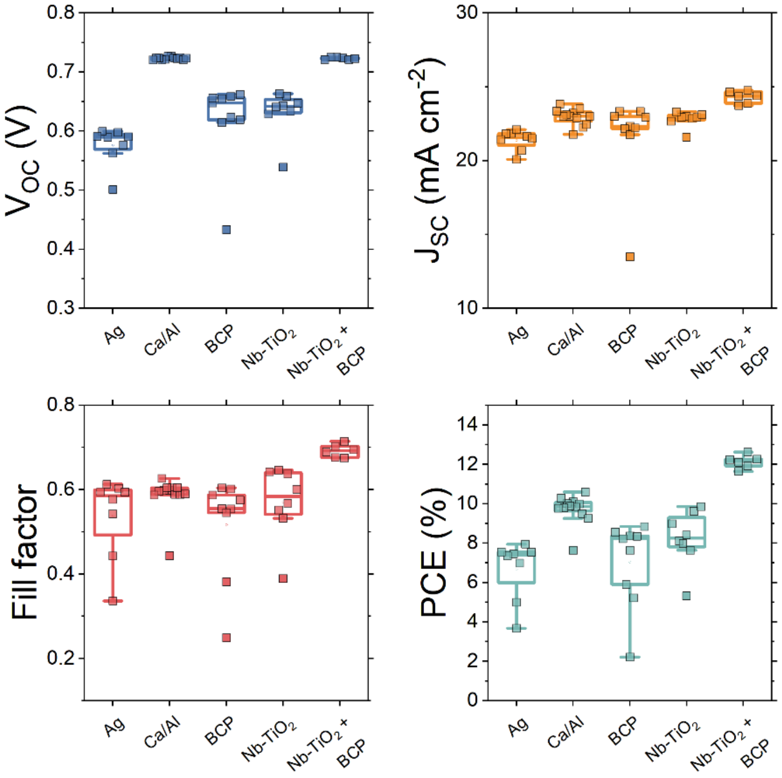

Figure S21. Current-voltage parameters for PTB7-Th : IEICO-4F organic solar cells employing interfacial layers between active layer and Ag electrode Data from a total of 45 devices (8x Ag with no additional interfacial layer, 12x Ca+Al, 9x BCP+Ag, 8x Nb-TiO_2+Ag, 8x Nb-TiO_2 + BCP +Ag).

ITO | PEDOT:PSS | | ….	**J**J_{SC} (mA cm^{-2})	V_{OC} (V)	**FF**	**PCE** (%)
BHJ | Ag	22.1	0.576	0.62	7.9
BHJ | Ca | Al	23.8	0.722	0.59	10.3
BHJ | **BCP** | Ag	22.9	0.656	0.58	8.8
BHJ | **Nb-TiO**$_2$ | Ag	23.1	0.648	0.63	9.3
BHJ | **Nb-TiO**$_2$ | **BCP** | Ag	24.8	0.724	0.72	12.6

Table S2. Current-voltage statistics for OPV devices employing different interfacial layers. The bulk heterojunction was comprised of a PTB7-Th (PCE10) donor polymer and IEICO-4F small molecule acceptor.

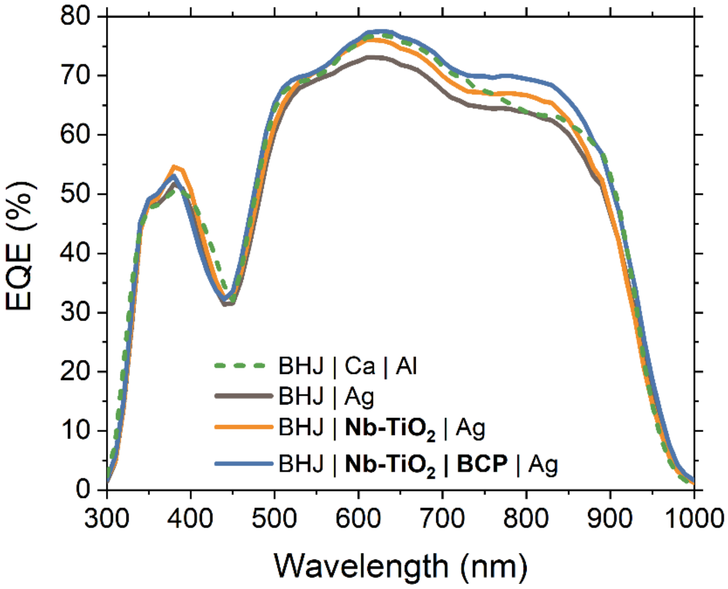

Figure S22: External quantum efficiency (EQE) measurement for organic photovoltaics (PTB7-Th & IEICO-4F) employing different interfacial layers between the bulk heterojunction (BHJ) and Ag electrode.

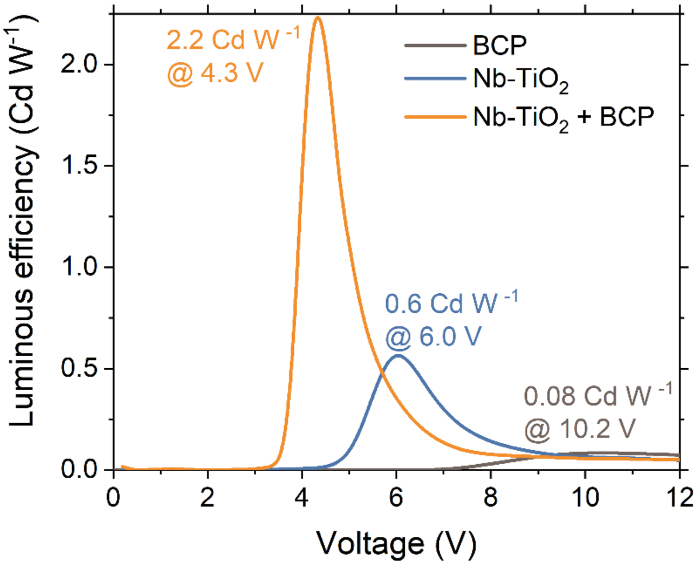

Figure S23: Luminous efficiency as a function of applied voltage for OLEDs employing different interfacial layers between organic emitter (F8:F8BT) and electrode (Ag).

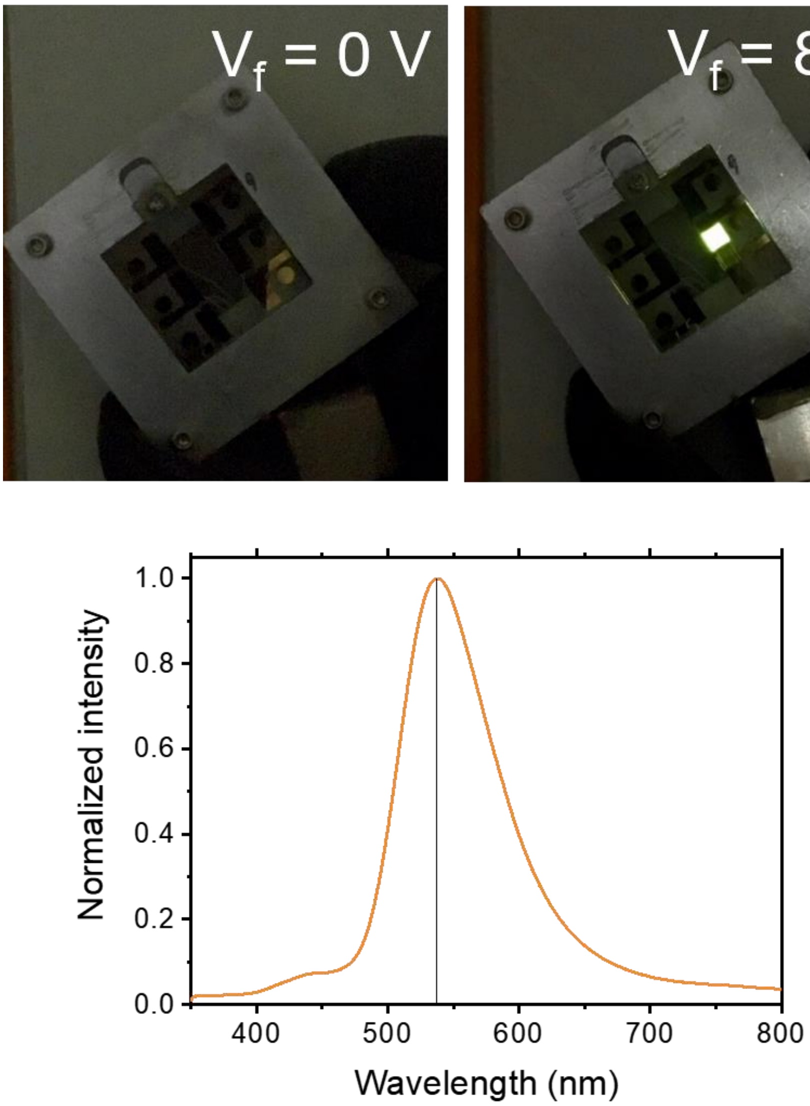

Figure S24. Photographs showing an F8:F8BT OLED employing a Nb-TiO_2 + BCP electrode bilayer interface at 0V and 8V forward bias as well as the emission spectra of the OLED with an intensity peak at 537nm.

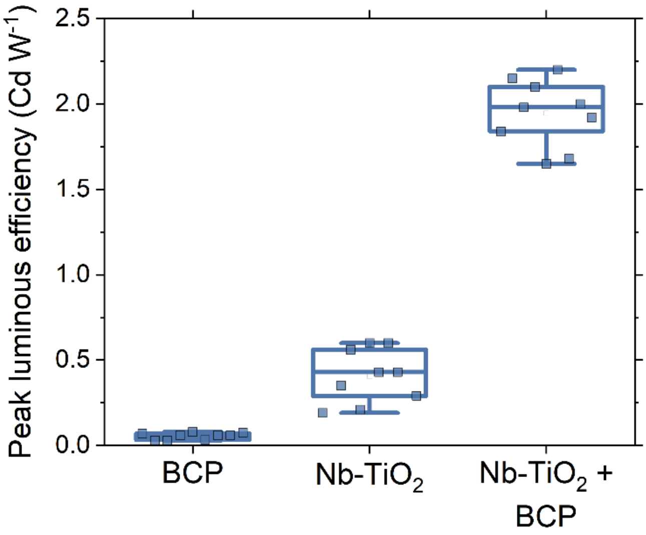

Figure S25. Statistical account of peak luminous efficiency for OLEDs employing different interfacial layers between F8:F8BT and Ag electrode. Data from 27 devices is shown (8 per variation).

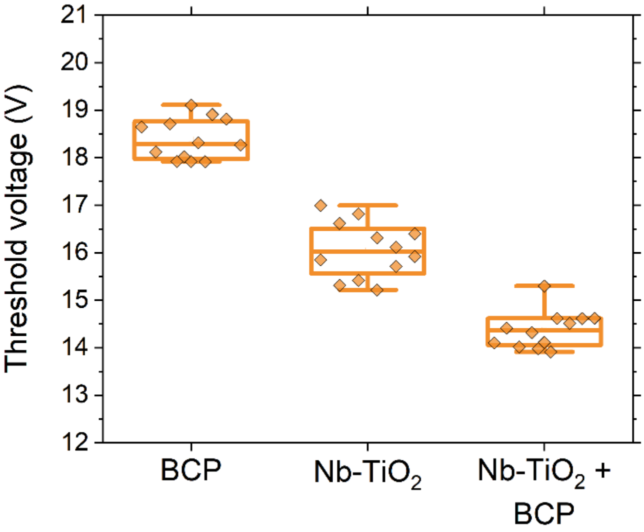

Figure S26. Statistical account of threshold voltage for TFTs employing different interfacial layers between ZnO and Ag electrode. Data from 36 devices is shown (12 per variation).

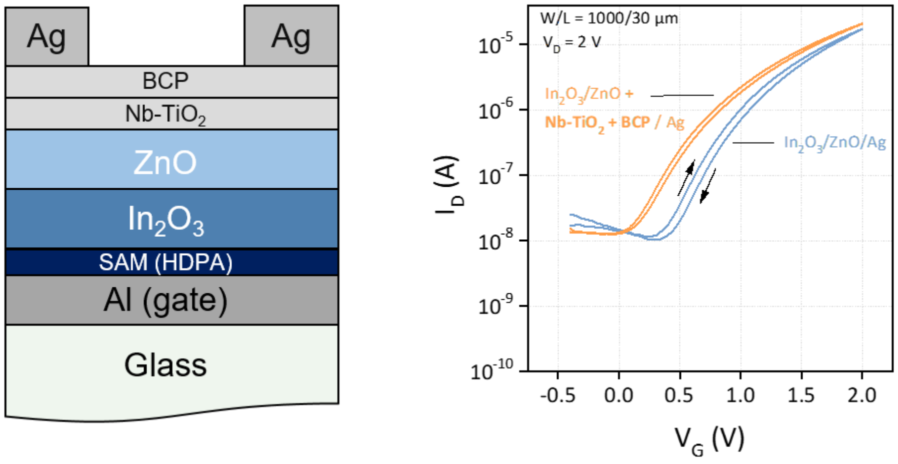

Figure S27. SAM-adsorbed gate thin-film transistor structure and I-V performance for device employing the Nb-TiO$_2$ + BCP bilayer interface. Similar to the device shown in Figure 6c, f, turn-on voltage is dramatically reduced upon the introduction of this bilayer.

References

1 P. Giannozzi, S. Baroni, N. Bonini, M. Calandra, R. Car, C. Cavazzoni, D. Ceresoli, G. L. Chiarotti, M. Cococcioni, I. Dabo, A. Dal Corso, S. De Gironcoli, S. Fabris, G. Fratesi, R. Gebauer, U. Gerstmann, C. Gougoussis, A. Kokalj, M. Lazzeri, L. Martin-Samos, N. Marzari, F. Mauri, R. Mazzarello, S. Paolini, A. Pasquarello, L. Paulatto, C. Sbraccia, S. Scandolo, G. Sclauzero, A. P. Seitsonen, A. Smogunov, P. Umari and R. M. Wentzcovitch, *J. Phys. Condens. Matter*, , DOI:10.1088/0953-8984/21/39/395502.

2 A. M. Rappe, K. M. Rabe, E. Kaxiras and J. D. Joannopoulos, *Phys. Rev. B*, 1990, **41**, 1227–1230.

3 J. P. Perdew and Y. Wang, *Phys. Rev. B*, 1992, **45**, 13244–13249.

4 M. Valiev, E. J. Bylaska, N. Govind, K. Kowalski, T. P. Straatsma, H. J. J. Van Dam, D. Wang, J. Nieplocha, E. Apra, T. L. Windus and W. A. De Jong, *Comput. Phys. Commun.*, 2010, **181**, 1477–1489.

5 A. D. Becke, *J. Chem. Phys.*, 1993, **98**, 5648–5652.

6 P. J. Stephens, F. J. Devlin, C. F. Chabalowski and M. J. Frisch, *J. Phys. Chem.*, 1994, **98**, 11623–11627.

7 N. Godbout, D. R. Salahub, J. Andzelm and E. Wimmer, *Can. J. Chem.*, 1992, **70**, 560–571.

8 K. Momma and F. Izumi, *J. Appl. Crystallogr.*, 2011, **44**, 1272–1276.

9 M. Saliba, J. P. Correa-Baena, C. M. Wolff, M. Stolterfoht, N. Phung, S. Albrecht, D. Neher and A. Abate, *Chem. Mater.*, 2018, **30**, 4193–4201.

10 W. Zhang, J. Smith, R. Hamilton, M. Heeney, J. Kirkpatrick, K. Song, S. E. Watkins, T. Anthopoulos and I. McCulloch, *J. Am. Chem. Soc.*, 2009, **131**, 10814–10815.

Supplementary Information